RSC Advances

PAPER

View Article Online
View Journal | View Issue

Cite this: *RSC Adv.*, 2024, **14**, 15862

Adsorptive removal of norfloxacin from aqueous solutions by Fe/Cu CNS-embedded alginate–carboxymethyl cellulose–chitosan beads†

Geetha Gopal and Amitava Mukherjee *

The pervasive application of pharmaceuticals in aquatic environments has acquired much focus owing to their nonbiodegradability and eco-toxicity, which might readily destroy the ecological balance. Developed chitosan–coated Fe–Cu CNS alginate–CMC beads (NBs) were utilized in this study to adsorb the quinolone antibiotic norfloxacin (NOR) from water for the first time. Under ideal conditions (C_{NOR}: 20 mg L^{-1}; sorbent conc.: 2000 mg L^{-1}; sorbent dosage: 0.15 g; interaction time: 300 min; solution pH: 6.0), about 86% NOR removal was achieved through batch mode. The removal performance for NOR was examined concerning pH, ionic strength, and coexisting micropollutants. The greatest NOR removal was attained on NBs with the greatest Langmuir adsorption capacity of 355 mg g^{-1} due to numerous mechanisms such as sorbent pore filling, electrostatic attraction, π–π attraction and hydrogen bonding. Studies using environmentally significant algae, such as *Scenedesmus* sp., to analyze the residual toxicity of treated NOR solution revealed a significant reduction in their toxic effects. Current research has demonstrated that nanocomposite beads are an excellent wastewater treatment material with promising industrial applications due to their ease of synthesis, exceptional surface adsorption properties, stability, and environmentally friendly reaction.

Received 14th March 2024
Accepted 12th May 2024

DOI: 10.1039/d4ra01971g

rsc.li/rsc-advances

1. Introduction

The first quinolone-related antibacterial agent to be developed and commercialized was norfloxacin (NOR). Because of its remarkable broad-spectrum antibacterial activity, it is frequently utilized in clinical treatment and agriculture. Fluoroquinolone (FQ) antibiotics, particularly norfloxacin, have been observed to be widespread in hospital wastewater. In European countries, researchers have detected these quinolone antibiotics in hospital sewage at concentrations ranging from 3 to 87 mg L^{-1}.[1] According to the recent data, the consumption of NOR has increased to 53 800 tons per year, leading to a significant rise in NOR discharges into water resources through various routes. High residual concentrations of these compounds, up to 31 mg L^{-1}, have been detected in water treatment plants in India due to the high use of generic antibiotics.[2] NOR and CIP were detected in Indian surface water, with maximum concentrations of 0.52 mg L^{-1} and 6.5 mg L^{-1}, respectively, in a binary mixture.[3] Additionally, studies conducted in Europe and America have also reported the presence of norfloxacin in streams and wastewater. Although the amount of norfloxacin detected is small, it may build up in the environment and harm the food chain.[4] Consuming water contaminated with undesirable NOR can result in various side effects and toxicity in humans. The most common toxic effects of this antibiotic include seizures, angioedema, peripheral neuropathy, tendon rupture, hallucinations, vomiting, nausea, diarrhoea, hypersensitivity responses, photosensitivity, Stevens–Johnson syndrome, prolongation of the QT interval, and an impact on the central nervous system.[4,5] Three factors contribute to the risks of NOR in wastewater: (1) The wastewater treatment plant's ability to remove non-organic pollutants (NOR) is restricted; average NOR removal effectiveness in wastewater treatment plants is reportedly just 68%. (2) Drug-resistant strains will evolve due to NOR entering the environment. (3) NOR is hazardous for numerous aquatic animals. Quick exposure to NOR halted the gut microbiota homeostasis of juvenile Pseudosciaena crocea. It was demonstrated that NOR exposure decreases metabolic, cellular, and information-processing pathways from a functional prediction analysis perspective.[6] The eradication of NOR from wastewater was investigated employing a range of wastewater treatment methodologies, encompassing adsorption, membrane filtration, adsorption-photocatalysis, coagulation, electrocoagulation, photo-Fenton, photocatalysis, and sonocatalysis. The membrane separation technique is expensive and prone to fouling. Large-scale operations are limited in their use of catalysts due to their high cost, and it can be difficult to determine whether the by-products of catalysis are harmful.[7] Adsorption is

Centre for Nanobiotechnology, VIT, Vellore, Tamil Nadu, India. E-mail: amit.mookerjea@gmail.com; amitav@vit.ac.in; Tel: +91 416 220 2620

† Electronic supplementary information (ESI) available. See DOI: https://doi.org/10.1039/d4ra01971g

the most desirable method among the alternatives in terms of its economic feasibility. Adsorption has several benefits over alternative methods for removing antibiotics from aqueous systems. These include ease of operation, high removal efficiency, versatility across a wide range of sorbate concentrations, and cost savings on instrumentation.[8] Activated carbon materials and inorganic minerals are the two general categories of adsorbents employed for NOR removal. It states that the activated carbon fibre experienced excellent adsorption ability to NOR. On the other hand, inorganic minerals have a relatively high thermal stability; recycling them through pyrolysis of NOR adsorbed on them may be simpler. Amid the many inorganic minerals, the inorganic layered materials—such as bentonite, hydrotalcite, brucite, and others—have drawn much attention lately because they typically show good antibiotic selectivity and adsorption performance.[9] Various adsorbents have been studied for the removal of NOR. Liu *et al.* used multi-doped porous carbon with a large surface area of 2299.7 $m^2\ g^{-1}$, which resulted in a high adsorption capacity of 917.43 mg g^{-1}.[10] In a separate study, honeycomb lignin-based biochar was utilized, achieving an NOR adsorption capacity of 519 mg g^{-1} with a surface area of 1537 $m^2\ g^{-1}$.[11] On the other hand, Cao *et al.* used a bentonite-enhanced sludge biochar with a much lower surface area of 40.61 $m^2\ g^{-1}$, resulting in a significantly lower adsorption capacity of 89.36 mg g^{-1}.[12] Interestingly, low-porous adsorbents can also be effective alternatives for NOR removal. Tang *et al.* investigated the use of alginate/chitosan composite hydrogel spheres with a specific surface area of 20 $m^2\ g^{-1}$, which showed a remarkable adsorption capacity of 310.6 mg g^{-1}, surpassing that achieved by MCM-41 molecular sieves (117 mg g^{-1}) with a much larger surface area of 1028 $m^2\ g^{-1}$.[13] Based on reports, the electrostatic interaction and weak van der Waals force are responsible for the binding interaction of bentonite clay interlayer spacing. This layered clay can be readily exfoliated by ultrasonic exfoliation to form a monolayer or multilayer nanosheets with strong hydration swelling properties. Consequently, the numerous adsorption sites of clay nanosheets (CNS) become visible, leading to a significant increase in adsorption efficiency. However, after adsorption, CNS are challenging to recover from water, which eventually limits their industrial uses. An effective strategy to address this issue was presented by creating three-dimensional (3D) structured CNS-based adsorbents.[14]

Biopolymeric materials and polysaccharides have emerged as the best options for wastewater purification when considering economic factors. Naturally occurring biopolymers, such as cellulose, chitosan, and alginate, have demonstrated impressive properties and an affinity for pharmaceutical pollutants. Although chitosan exhibits excellent antibiotic adsorption properties, it is limited by its mechanical strength. This limitation can be overcome by cross-linking it with cellulose, allowing the stiffness of cellulose to support and reinforce the adsorbent thermally and mechanically. Alginate can form hydrogel beads by cross-linking with Ca^{2+} ions and contains surface-OH groups that can attract complex antibiotic molecules. Combining cellulose, chitosan, and alginate produces a composite adsorbent that addresses their stability issues.[15] It was reported that cellulose, chitosan, and clay-based nanocomposites are effective adsorbents for removing antibiotics, which has motivated the exploration of these readily available and natural polymers for use in NOR adsorption The addition of metal–clay nanocomposite to the hydrogel beads enhances the removal efficiency of the adsorbent from an aqueous system by utilizing catalytic efficiency with high clay adsorption properties while maintaining the stability of the composite in the hydrogel form. Hence, in the present study, chitosan, sodium alginate, and carboxymethyl cellulose have been chosen because of their non-toxic nature, economical, abundant, eco-friendly, and biodegradable properties for developing Fe–Cu CNS-loaded hydrogel beads.[16]

Additionally, compared to multilayered clay materials, the exfoliated clay nanocomposite produced through the intercalation of metal nanoparticles could possess a higher specific surface area and binding ability, both of which aid in achieving improved adsorption performance.[17] According to this theory, the synthesis of bimetallic nano-composites began with the exfoliation of clay to take advantage of the unique qualities of bentonite clay, including its high cation exchange capacity, swelling, and widespread availability.[18] Ahmed *et al.*, 2023, reported that ciprofloxacin and levofloxacin were removed from the contaminated medium using green synthesized Fe–Cu/Alg–LS (Fe–Cu supported on alginate–limestone) as an adsorbent, with a maximum removal efficiency of 97.3% and 100%, respectively.[19] Hence, in the previous research, we designed chitosan–coated CNS supported by Fe–Cu nanocomposite-loaded alginate–CMC beads to effectively remove ciprofloxacin with a removal percentage of 117.65 mg g^{-1}.[20] Therefore, the effectiveness of the nanocomposite beads in removing antibiotics against NOR was investigated in this study.

The main goals included (1) detailed study on surface morphology, thermal stability, and elemental composition of NBs using FESEM-EDX, TGA/DTA, and XPS analysis (2) carrying out a study on batch removal to examine the operational parameters such as bead loading, bead weight, different sorbent, impact of coexisting ions and solution pH (3) thermodynamics studies, kinetics analysis, and analysis of adsorption isotherms to explain possible adsorption mechanisms (4) using FT-IR, XRD, HRLC-MS, and TOC analysis to characterize the NBs before and following NOR adsorption; (5) evaluating the treated NOR solution's suitability for real-world wastewater remediation, as well as its residual toxicity and reusability.

2. Materials and methods

2.1 Materials used

Chitosan (degree of deacetylation ≥ 75%, viscosity 20–300 cps), anhydrous calcium chloride granules (7.0 mm, 93.0%), ferric chloride hexahydrate (ACS reagent, 97%), montmorillonite, cupric chloride dihydrate (ACS reagent, ≥ 99.0%) were purchased from Sigma-Aldrich, Mumbai, India. Sodium alginate (pure) from Sisco laboratories, Chennai and carboxymethyl cellulose from Molychem, Mumbai, were obtained. Norfloxacin ($C_{16}H_{18}FN_3O_3$, Analytical standard, ≥98%) purchased from Merck, Mumbai. Distilled deionized water (Millipore system)

was used in all experiments, and all other chemicals were directly utilized with no additional purification.

2.2 Nanocomposite beads preparation

2.2.1 Preparation of nanocomposite. The formation of nanocomposite Fe/Cu CNS mainly involves two steps. In the first step, CNS were prepared using the ultrasonication technique. In the second step, Fe/Cu bimetallic nanoparticles were dispersed over the CNS surface by *in situ* reduction technique. The preparation technique has been elaborated in the ESI (ESI 1).†

2.2.2 Encapsulation of nanocomposite Fe/Cu CNS alginate–carboxymethyl cellulose–chitosan beads (NBs)

2.2.2.1 Solution A. Sodium alginate–CMC mixture was prepared by dissolving 5 wt% of sodium alginate and 2 wt% CMC in 100 mL of distilled deionized water. The solution was heated at 40 °C until the solution became clear.

2.2.2.2 Solution B. Different mass ratios of nanocomposite (100, 500, 1000 and 2000 mg L^{-1}) were sonicated in a probe sonicator and added to solution A to formulate solution B. Subsequently, solution B was carefully added drop by drop to the 2wt% $CaCl_2$ solution to initiate bead formation.

2.2.2.3 Solution C. Chitosan (1 wt%) was dissolved in the glacial acetic acid to get solution C. The prepared beads were soaked in solution C to obtain the Fe/Cu CNS alginate–carboxymethyl cellulose–chitosan beads (nanocomposite beads (NBs)). Further, the beads were washed and dried in the vacuum oven overnight and stored in the desiccator.

2.3 Characterization study

The Field Emission Scanning Electron microscope (FE-SEM, Thermo Fisher FEI QUANTA 250 FEG), in combination with Energy Dispersive Spectroscopy (EDS), was used to characterize the NBs. The instrument is equipped with a Schottky Field Emission Electron Gun, which serves as a source of electrons, with an operating voltage range of 5–30 kV. It offers a high resolution of 1.2 nm at 30 kV under high vacuum conditions. The instrument uses the Everhart Thornley detector. Fourier-transform infrared (FT-IR) spectra were acquired with a JASCO FT/IR-6800 spectrometer using the attenuated total reflection (ATR) method. The spectral range was recorded from 4000 to 400 cm^{-1} with an accuracy of 4 cm^{-1}. OriginPro 2023 software from OriginLab Corporation was utilized to process the data. The transmission bands associated with the secondary structure were identified based on relevant literature. A Bruker D8 Advance X-ray powder diffractometer from Germany was utilized to obtain XRD patterns of NBs both before and after NOR interaction. The scanning range was set from 10° to 100° using Cu K radiation at 40 kV and 40 mA with a 2.2 kW Cu anode, Lynx Eye detector, and Ni filter. The antibiotics were measured using a UV-visible spectrophotometer (U-2910 spectrophotometer, Hitachi, Japan). A total organic carbon (TOC) analyzer (Model TOC-L, Shimadzu, Japan) was used to track changes in the organic carbon content of the treated NOR solution. Orbitrap-High Resolution Liquid Chromatograph Mass Spectrometer (O-HRLCMS) (Q-Exactive Plus Biopharma, Thermo Scientific); (column details: syncronis-C18 100 × 2.1 mm, 1.7 microns; solvent A: 0.1% formic acid in Milli-Q water, solvent D: acetonitrile; flow rate: 0.3 mL min^{-1}, column temperature: 35 °C) was used to identify secondary metabolite products created as a result of antibiotic interaction with NBs.

2.4 Adsorption experiments

100 mg of NOR was added to 500 mL of distilled deionized water and kept overnight, stirring to produce 200 mg L^{-1} of stock solutions, which was stored at 4 °C in the refrigerator and used to prepare all the test solutions in this work. Batch studies of NOR removal from the aqueous system by adsorption on the NBs were performed. The experiments were conducted in the 50 mL falcon tubes with the parameters of various bead loading, bead weight and different sorbent effects. The tubes were continuously stirred in an orbital shaker at a speed of 100 rpm. The NBs were removed from the test solution once the equilibrium state was reached, and the solution was then filtered using a 0.45-micron filter to measure the NOR content using UV-vis spectroscopy (U-1672910 spectrophotometer, Hitachi, Japan) at 276 nm and the residual concentration of NOR was determined by substituting into the standard curve (provided in ESI 4 (Fig. S4) file†) with the regression value (R^2) = 0.97.The calculated detection limit of NOR (LOD) in the aqueous system is 2.72 mg L^{-1}, and the Limit of Quantification (LOQ) is 8.24 mg L^{-1}. The amount of NOR adsorbed was determined as the difference between its initial and final concentration in solution. NOR stability and adsorption on vials were assessed by analyzing blanks of NOR in deionized water. All experiments were carried out in triplicate under the optimized condition, and the average values were presented.

The NOR removal percentage and removal capacity of NBs are given below,

$$\text{NOR } (R\%) = (C_0 - C_t/C_0) \times 100 \quad (1)$$

$$q_e = \frac{(C_0 - C_t)}{m} \times V \quad (2)$$

Here, q_t (mg g^{-1}) represents the quantity of NOR adsorbed by the NBs at time (min), where C_0 and C_t (mg L^{-1}) denote the initial and residual concentrations of NOR at time t, respectively. V (L) and m (g) signifies the volume of the NOR solution and mass of the NBs employed.

A comprehensive understanding of the pH's influence on NOR removal and its adsorption kinetics, isotherms, and thermodynamics is crucial for elucidating the primary factors governing NOR adsorption and the associated mechanisms. The effect of environmental factors (salts, humic acid, and microplastics) on NOR removal was studied using the effective bead loading and weight determined from the initial experiments.

2.4.1 Effect of pH. 0.3 g of NBs was contacted with 20 mg L^{-1} of NOR solution (200 mL) for 300 min. The pH of this solution varied between 2.0 to 10.0 by adding the required amounts of 0.1 M HCl or NaOH aqueous solution.

2.4.2 Adsorption kinetics. 0.30 g of NBs was added into 200 mL of NOR solution (20 mg L^{-1}, neutral pH) in a 250 mL screw cap bottle. Subsequently, the samples were vibrated for

varying intervals (30, 60, 90, 120, 150, 180, 210, 240, 270 and 300 min) at 100 rpm to determine the residual NOR concentration.

2.4.3 Adsorption isotherm and thermodynamics. The same procedures were followed for the thermodynamic and isotherm studies. Isotherm investigations were carried out by applying different NOR concentrations (10 to 100 mg L^{-1}) with 300 min of contact time at room temperature. Thermodynamic analyses were conducted using 20 mg L^{-1} of NOR solution for 300 min with varying temperature ranges of 288, 298, and 308 K, respectively.

2.4.4 Effect of environmental parameters. To examine the impact of ionic strength on NOR adsorption, the concentrations of NaCl and $CaCl_2$ in a 20 mg L^{-1} NOR solution were adjusted in the range of 0.05 to 1.0 M, respectively. Subsequently, 3.0 mg of NBs was introduced into each 20 mL NOR solution, and the residual NOR was measured following an equilibration period of 300 min. The influence of HA on NOR removal was assessed by varying the dosage of humic acid (HA) in the NOR solution by 1, 2, 3, 4, and 5 M. The influence of microplastics was examined by introducing different amounts of polyethylene (PE, 12 μm, 1–5 M) into a solution volume of 20 mL with a concentration of 20 mg L^{-1} of antibiotic (NOR) along with adsorbents. After reaching adsorption equilibrium, the residual NOR concentration was ascertained, and the removal capacity was assessed.

2.5 Environmental sustainability test

2.5.1 Reusability study. A series of adsorption and desorption tests were conducted to investigate reusability. The treated NBs was washed after the equilibrium adsorption and oscillated for 12 hours while immersed in a 0.1 M HCl solution. Subsequently, it underwent three rinses with deionized water after elution. After that, the desorbed NBs were put through another cycle of adsorption and desorption.

2.5.2 Toxicity study. The method used for toxicity testing has been modified from our earlier studies. The freshwater algal strain *Scenedesmus* sp. was cultured in BG-11 medium for 15 days at 20 °C in a day–night cycle. The toxicity of the treated NOR solution was examined on the harvested algae in their exponential growth phase. To obtain an algal pellet for the toxicity test, the grown algal cells were centrifuged at 7000 rpm for 10 minutes and then washed with filtered lake water. The separated algal cells of 0.5 OD interacted with NOR, treated-NOR and treated-stimulated hospital effluent for 72 h. The interacting samples were subjected to an MTT assay on day 3 to assess the toxicity of the treated NOR solution.

2.5.3 Effect on real water samples. The NOR removal studies from different sources of water (tap, ground, and lake) aimed to show the efficiency of the NBs against antibiotic pollutants in water ecosystems. Samples of tap water, lake water, and groundwater (12°97′14.4″N, 79°16′63.5″E; 12°96′88.2″N, 79°15′91.5″E; and 12°96′81.7″N, 79°16′03.7″E, respectively) were taken from the VIT University campus, Vellore and adulterated with 20 mg L^{-1} of NOR for the removal study.

2.5.4 Effect on stimulated hospital effluent. To investigate the efficiency of the NBs for the treatment of actual wastewater simulated hospital effluents have been generated by mixing various pharmaceuticals, carbohydrates, and other inorganic and organic compounds that are frequently found in actual waste from healthcare facilities. The compounds are listed along with their concentrations in Table S1, ESI Material.†

3. Results and discussion

3.1 NBs characterization study

The technique for the synthesis and development of nanocomposite beads was given in the ESI 1† file and the schematic representation of NBs formation was given in Fig. S1.† The ESI 2† provides the experimental procedure for measuring the surface charge (pH_{PZC}) of NBs. In our earlier study, we confirmed the synthesized Fe/Cu CNS and NBs using FTIR, XRD, and SEM-EDX and the detailed characterization analysis was given in the ESI 3 file (Fig. S2 and S3).† The NBs were uniform spheres with an average diameter of 2 mm, with a rough and dense surface that improves the number of adsorption sites available. Adding the nanocomposite enhances the pore volume and SSA of the control beads. Furthermore, the FTIR spectrum of the Fe/Cu CNTs and NBs showed oxygen-containing functional groups on the surface of NBs, which play an important role in NOR adsorption through hydrogen bonding. XRD study confirmed the crystal structure of the developed NBs, which matched those of Fe/Cu CNS nanocomposite, offering strong proof of the effective loading of nanocomposite within the hydrogel beads.[20]

The TGA cure (Fig. 1) gives the changes in the weight loss of NBs with temperatures up to 800 °C. The NBs exhibited three zones of mass loss. The first stage, attributed to water loss within the material, the zone corresponding to a 20% weight loss occurred at temperatures below 200 °C. The second stage, which corresponds to the primary decline in weight (55%) from 300 to 450 °C, is attributed to cellulose, alginate, and chitosan degradation. The third thermal phase, linked to the decomposition of

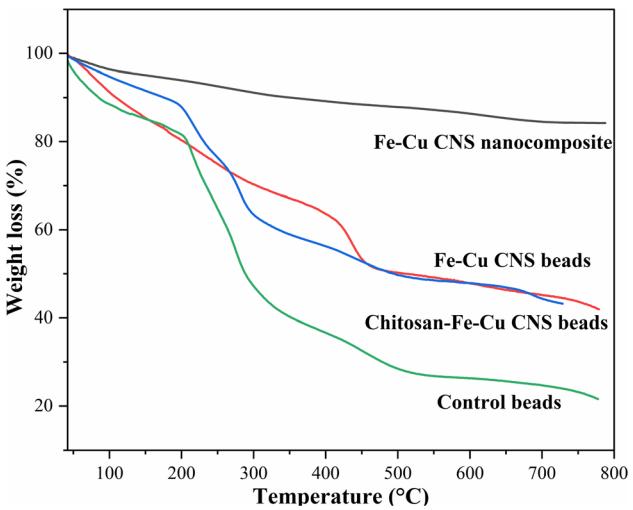

Fig. 1 TGA analysis of Fe/Cu CNS, Fe/Cu CNS beads, chitosan–Fe/Cu CNS beads, control beads.

the sample, initiates at 450 °C, and causes a 25% reduction in weight. It has been established that adding clay improves NBs' thermal stability. As a result, it was determined that the thermal stability threshold of NBs was roughly 300 °C.[21,22]

3.2 Adsorption experiments

In the adsorption process, the NBs' weight, loading, and types of sorbents greatly affect the adsorption efficiency.20 mL of NOR solution (20 mg L^{-1}) was mixed with 0.01–0.2 g L^{-1} of NBs to test the effect of adsorbent weight at 298 K (ESI 5†). Fig. S5a† illustrates the increasing trend in the adsorbent removal rate on NOR as the number of adsorbent increases. The rate of NOR removal experienced a significant increase, rising from 50% to 87%, with the increment of NBs weight from 0.01 g L^{-1} to 0.2 g L^{-1}. An increase in the quantity of adsorbent creates numerous active sites for NOR, facilitating the removal of NOR from the solution. The NOR in the solution was completely adsorbed when there was sufficient adsorbent present, and the removal rate gradually increased.[23]

The effect of NB dosage was studied to find the most cost-effective point in the NOR adsorption process. The adsorption experiments conducted in batches involved using a bead weight of 0.15 g, NOR concentration of 20 mg L^{-1}, and a pH of 6.0. The adsorption rate increased as the amount of composite was increased from 500 to 2000 mg L^{-1}, as Fig. S5b† illustrates. This finding may be attributed to the presence of available active sites on the easily accessible composite surface. On the other hand, when the quantity of adsorbents is minimal, adsorption may reach saturation and all of the adsorbent's active sites are exposed in the NOR solution; as a result, the adsorption capacity increases.[24]

To compare the adsorption effectiveness of Fe/Cu CNS, alginate–CMC–Fe/Cu CNS, chitosan–coated alginate–CMC–Fe/Cu CNS, and control bead for NOR removal, 20 mg L^{-1} of NOR solution treated with 0.15 g of NBs at 298 K. According to Fig. S5c,† the order of the NOR's adsorption capacity was Fe/Cu CNS > control bead > alginate–CMC–Fe/Cu CNS > chitosan coated alginate–CMC–Fe/Cu beads. Fewer active adsorption functional groups may cause the nanocomposites and the control bead's comparatively low adsorption capacity towards NOR. Since NBs have a higher specific surface area than nanocomposite and, therefore, more sites for adsorption, they have a superior adsorption capacity.[25]

3.2.1 Effect of pH. pH plays a crucial role in determining the interaction between NBs and NOR by influencing the surface charges of NBs and the ionization of functional groups in NOR. The NOR adsorption was investigated across a pH range of 2.0 to 10.0 to assess pH-related effects (Fig. 2a). At pH levels ranging from 4.0 to 6.0, the NBs demonstrate a relatively effective adsorption capacity for NOR. The NOR adsorption efficiency rose to 67% when the pH levels were changed from 2.0 to 4.0. In contrast, the NOR adsorption drops to 30% when

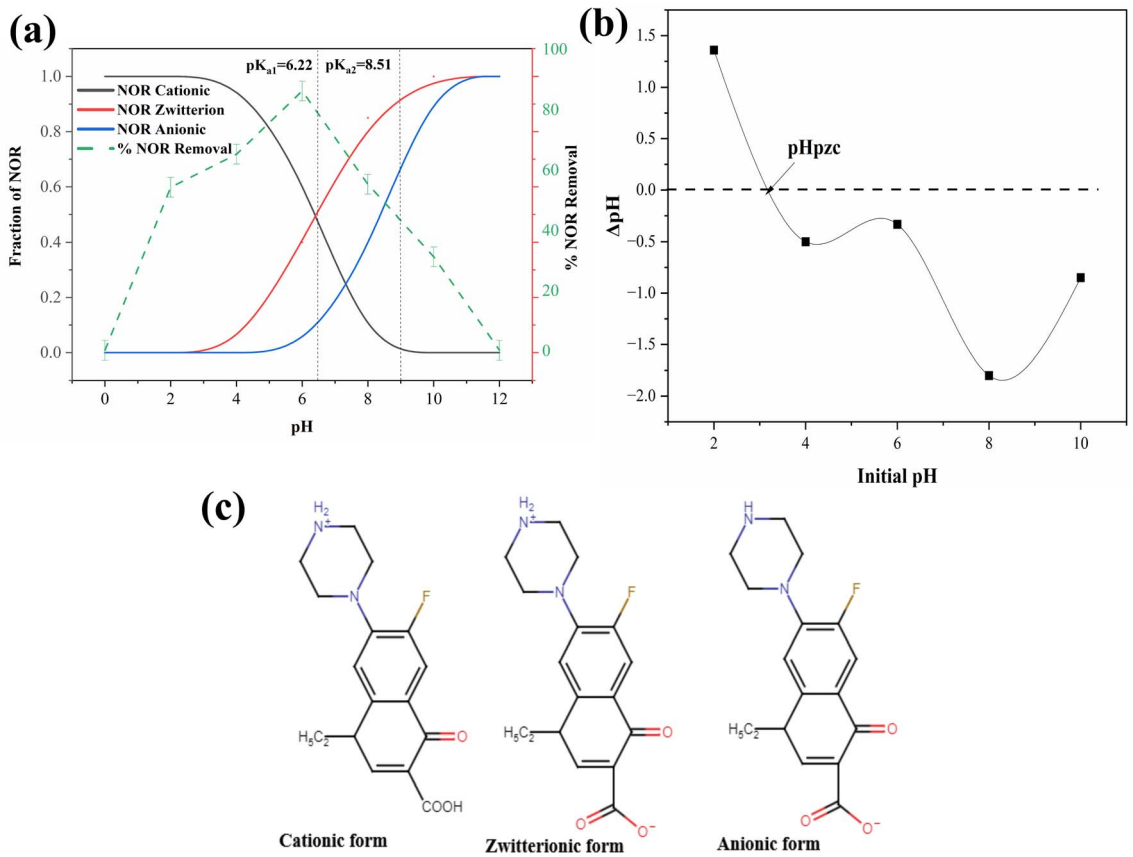

Fig. 2 (a) pH speciation of NOR and % NOR removal efficiency (b) surface charge of NBs (c) ionic forms of NOR.

the pH is raised from 6.0 to 10.0. These results could be influenced by electrostatic attraction.[26]

The adsorption process of NBs is influenced by their surface properties. At pH values below the point of zero charge (pH_{PZC}), which in this case is 4.2 (Fig. 2b), the electrostatic repulsion interaction between positively charged NBs and cationic NOR is strengthened, resulting in diminished adsorption. Additionally, the competition between cationic NOR and H^+ for the adsorption sites may also hinder NOR adsorption. In contrast, when the pH falls within the range of pK_{a_1} > pH > pHpzc, the NBs acquire negative charges, and the electrostatic attraction between NBs and cationic NOR is enhanced, leading to increased NOR uptake. However, as the pH continues to rise to neutral and basic levels, the electrostatic attraction is weakened, and the electrostatic repulsion interaction between negatively charged NBs and NOR anions is intensified, causing adsorption to decrease. Therefore, pH should be taken into account when studying NOR adsorption on NBs.[27] At pH levels <6.22, >8.51, and between 6.22 and 8.51, NOR is present as a cation, an anion, and a zwitterion (Fig. 2c). With pH ranging from 2.0 to 6.0, the NOR adsorption rate increased due to the notably heightened positive surface charge of the NBs, leading to electrostatic attraction. As the pH increased, the NOR adsorption capacity declined from 6.0 to 10.0, this should be explained by the stronger electrostatic repulsion caused by a higher proportion of anionic NOR. These findings demonstrated that electrostatic attraction was the primary mechanism supporting NOR adsorption on NBs. The highest NOR removal rate in the investigated pH range was observed at pH 6.[28]

3.2.2 Adsorption kinetic study. It is of considerable importance to fit the experimental data using an adsorption kinetic model to investigate the adsorption mechanism. The experimental data on adsorption kinetics and appropriate NOR models on NBs are shown in Fig. 3a–c. Adsorption occurs quickly in the first stage, with a sharp rise in adsorption capacity. As the NBs-NOR adsorption continues, the removal

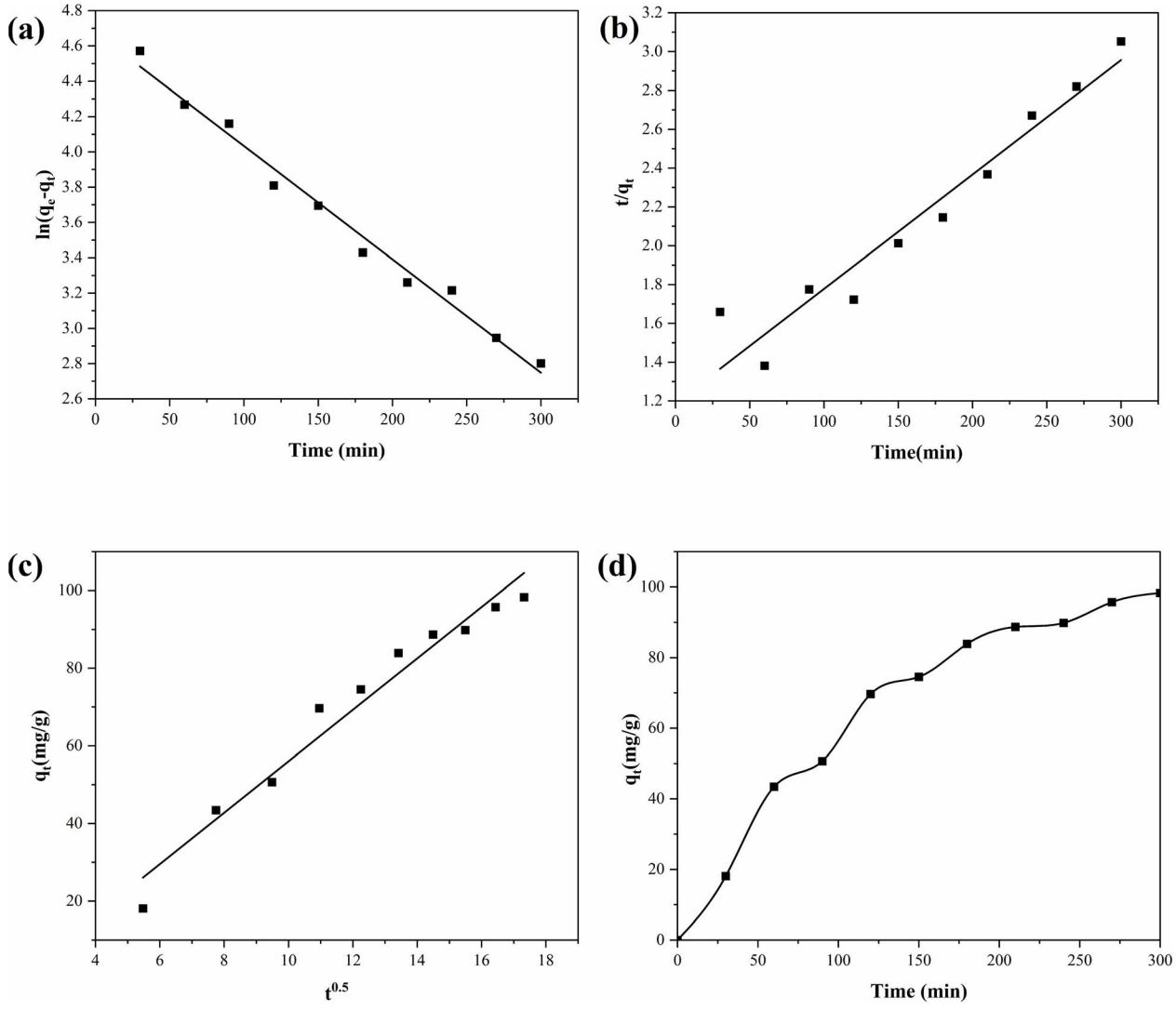

Fig. 3 Adsorption kinetic models (a) PFO model (b) PSO model (c) IPD model (d) NOR adsorption capacity (optimized condition: C_{NOR} 20 mg L^{-1}; C_{SOR} 0.15 g L^{-1}; pH 6; and contact time 300 min).

rate decreases, and the adsorption capacity increases gradually until the adsorption state attains equilibrium. The findings can be stated as follows: initially, the NOR molecules quickly fill the available adsorption sites on the NBs' surface; following this, the adsorption capacity of the NBs reaches its optimum level.[29]

The pseudo-first-order (PFO) kinetic model describes the physisorption reactions among adsorbent and adsorbate. The chemisorption interaction between the adsorbent and the adsorbate is explained by the pseudo-second-order (PSO) kinetic model. The mechanism behind the penetration of adsorbents and NOR is called intra-particle diffusion (IPD).[30] The expressions for the kinetic models are

$$\text{PFO: } \ln(q_e - q_t) = \ln q_e - K_1 t \quad (3)$$

$$\text{PSO: } \frac{t}{q_t} = \frac{1}{K_2 q_e^2} + \frac{t}{q_e} \quad (4)$$

$$\text{IPD: } q_t = K_D t^{\frac{1}{2}} + C \quad (5)$$

Table 1 Adsorption kinetics parameters

Kinetic models	NOR
Pseudo first-order	
q_e (mg g^{-1})	107.339
K_1 (min^{-1})	0.00002
R^2	0.986
Pseudo second-order	
q_e (mg g^{-1})	200
K_2 (mg g min^{-1})	0.000021
R^2	0.935
Intraparticle diffusion model	
K_d (mg g^{-1} min$^{-1/2}$)	6.625
C	10.25
R^2	0.963

The NOR adsorption capacity at equilibrium and any time point (min) are indicated by q_e (mg g^{-1}) and q_t (mg g^{-1}), respectively. The pseudo-first-order and pseudo-second-order kinetic model rate constants are related to k_1 (min^{-1}) and k_2 (g mg^{-1} min^{-1}), respectively. The intra-particle constant is k_D, and the kinetic constant for the IPD model is C.

Table 1 presents the data acquired from the kinetics investigation of NOR adsorption by NBs. Sorbent/sorbate reactions occurred on the solid surface, indicating that NOR adsorption onto NBs is physisorption, as supported by the correlation coefficient (R^2) showed that experimental findings were satisfactory with the PFO model.[31] Concerning the PSO and PFO, neither can differentiate the diffusion mechanism. The IPD model was used to analyze the diffusion mechanisms, yielding multi-linear plots exhibiting three stages, as depicted in Fig. 3c. The initial step explained how NOR molecules moved from an aqueous solution to the surface of NB's active sites. The subsequent phase is correlated to the NOR diffusion towards the inner surface of sorbent pores. In the third stage, equilibrium is attained between adsorption and micropore diffusion.[32]

3.2.3 Adsorption isotherm and thermodynamic study. The adsorption isotherm study shows the maximum adsorption capacity and the adsorption mechanism, which additionally demonstrates how NOR molecules are distributed throughout the adsorbent's porous media. Freundlich, Langmuir, and Temkin—three commonly employed isotherm models—were examined and discussed. The expressions for the non-linear isotherm models are

$$q_e = \frac{q_m K_L C_e}{1 + K_L C_e} \quad (6)$$

$$q_e = K_F C_e^{1/n} \quad (7)$$

$$q_e = \left(\frac{RT}{b_T}\right) \ln(K_T C_e) \quad (8)$$

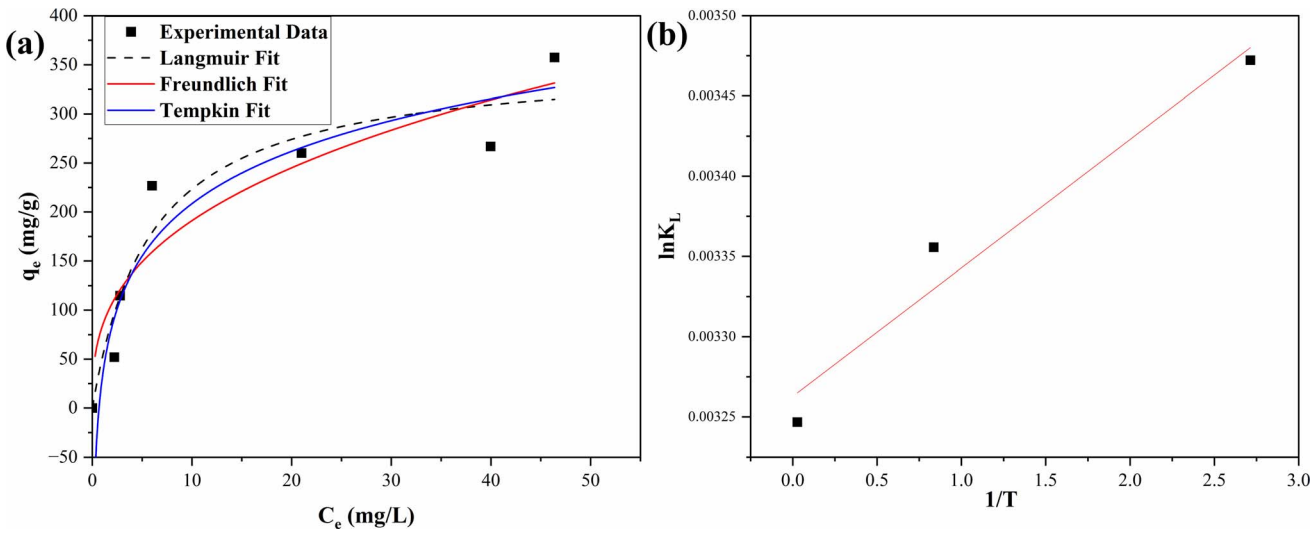

Fig. 4 (a) Adsorption isotherm (C_{NOR} = 10–100 mg L^{-1}; C_{SOR} 0.15 g L^{-1}; pH 6; and contact time 300 min) (b) thermodynamics (optimized condition: C_{NOR} 20 mg L^{-1}; C_{SOR} 0.15 g L^{-1}; pH 6; and contact time 300 min).

Table 2 Isotherm parameters

Isotherm models	Parameters	NOR
Langmuir	$q_{m,\ cal}$ (mg.g^{-1})	354.9 ± 41
	K_L	0.16 ± 0.07
	R^2	0.92
	R_L	0.238
Freundlich	n	2.77
	K_F	83.62 ± 29
	R^2	0.82
Temkin	b	77.13 ± 13
	K_T	1.49 ± 0.79
	R^2	0.92

C_e denotes the equilibrium NOR concentration (mg L^{-1}), and K_L indicates the Langmuir constant (L mg^{-1}). K_F (mg g^{-1} (L mg^{-1})) and n defines the Freundlich constant and heterogeneity factor. b and K_T referred to the Temkin constant. Fig. 4a shows the fitting of the isotherm model, and Table 2 provides the adsorption isotherm parameter. The R^2, determined from the Langmuir equation, was 0.92, which showed the best fit compared to the other 2 models. According to the Langmuir model, specific adsorbent sites are fully occupied by adsorbate molecules, forming a monolayer, and these adsorption sites are uniformly distributed across the surface of the adsorbent. These results showed that NOR has a maximum estimated adsorption capacity of 354.9 mg g^{-1} on NBs.[33] Furthermore, the dimensionless separation aspect (R_L), which demonstrated favorability of the process, can be expressed as

$$R_L = \frac{1}{1 + K_L C_0} \tag{9}$$

The derived R_L value of 0.238 indicates that the adsorption of NOR onto NBs is favorable. The Freundlich isotherm model gives the multilayer adsorbate sorption on the composites' heterogeneous surface. Utilizing the parameters obtained from the Freundlich model is beneficial for characterizing the adsorption behavior. The value of $1/n$ being <1 (0.358) suggests the favorability of the NOR adsorption process. In addition, the K_F value, which is approximately 83.62 ± 29, demonstrated the strength of NBs adsorption capacity.[34]

The thermodynamic behaviour of adsorption was examined to get a deeper understanding of the spontaneity of the NOR adsorption approach and calculation of inherent energy. The Van Hoff equation was used to calculate the changes in the following significant factors: the gibbs free energy (ΔG° (kJ mol^{-1})), the enthalpy (ΔH° (kJ mol^{-1})), and the entropy changes (ΔS° (kJ mol^{-1})). The equation follows,

$$\Delta G^\circ = -RT \ln\left(\frac{q_e}{C_e}\right) \tag{10}$$

The graph of $\ln K_L$ *vs.* $1/T$ values (linear plot) (Fig. 4b), ΔH° and ΔS° values were determined. Table 3 provides these thermodynamic variables. The gibbs free energy values exhibit negativity across all the temperatures examined, showing that NOR adsorption occurs onto NBs thermodynamically spontaneous and favorable. The positive ΔH° confirmed the endothermic nature of the NB adsorption reactions. Furthermore, ΔH° data lower than ΔH < 84 (kJ mol^{-1}) are indicative of physical adsorption; as a result, the ΔH° data obtained showed that NOR adsorption was a physical process, which is consistent with the findings derived from the ΔG° value. As a result, positive ΔS° values suggest an enhancement in the interaction between the solution containing NOR and the solid NBs interface.[35]

3.2.4 Effect of environmental factor. The ionic composition in real water and wastewater is intricate and exceedingly varying. Considering that the existence of ions can influence the degree of interaction between NBs and the target compound, the investigation focused on the effect of ionic strength on NOR adsorption. Na^+ and Ca^{2+} ions were selected for this study due to their widespread presence in various water sources. The impacts of these two major cations on the removal of NOR was shown in Fig. 5a. The adsorption removal percentage decreases with increasing ionic strength (86.07% to 16.59% for NaCl and 13.44% for $CaCl_2$). At pH 6, the NB's surface had a positive charge, and the NOR form was zwitterionic. As the ions compete for vacant binding sites on the surface of NBs and participate in cation exchange, the Na^+ and Ca^{2+}impede the NOR adsorption. Furthermore, the protons on the surface of the NBs will be partially displaced by the addition of Na^+ and Ca^{2+}, weakening the hydrogen bond between the NBs and NOR.[11]

MPs are a prevalent polymer contaminant found in many different aquatic systems. Additionally, studies have shown that MPs can bind on the adsorbents surface with a specific adsorption effect on other organic pollutants, specifically pharmaceuticals. For real-world application and treatment, the focus should be given to the problem of multifaceted contamination in the water and the concurrent presence of organic contaminants and MPs. To evaluate the impact of coexisting MPs on the NOR adsorption by the NBs, 20 mg L^{-1} of NOR solutions were mixed with varying concentrations of microplastic polyethylene (PE, 125 μm size). When the threshold concentration of NOR rises, the coexisting PE prevents NOR from attaching to the NBs surface, reducing the removal percentage shown in Fig. 5b. Following the adsorption of NOR in the presence of MP, the vacant active sites on the bead surface were obstructed by PE.[36]

HA, is a macromolecular organic material (mainly composed of π electrons) that is abundant in the natural world. It is necessary to investigate the impact of HA in the adsorption rate

Table 3 Thermodynamics parameters

	NOR		
Temperature [K]	ΔH° (kJ mol^{-1})	ΔS° (J mol^{-1} K^{-1})	ΔG° (kJ mol^{-1})
288	6.657×10^{-7}	0.027	−1.296
298			−0.929
308			−0.069

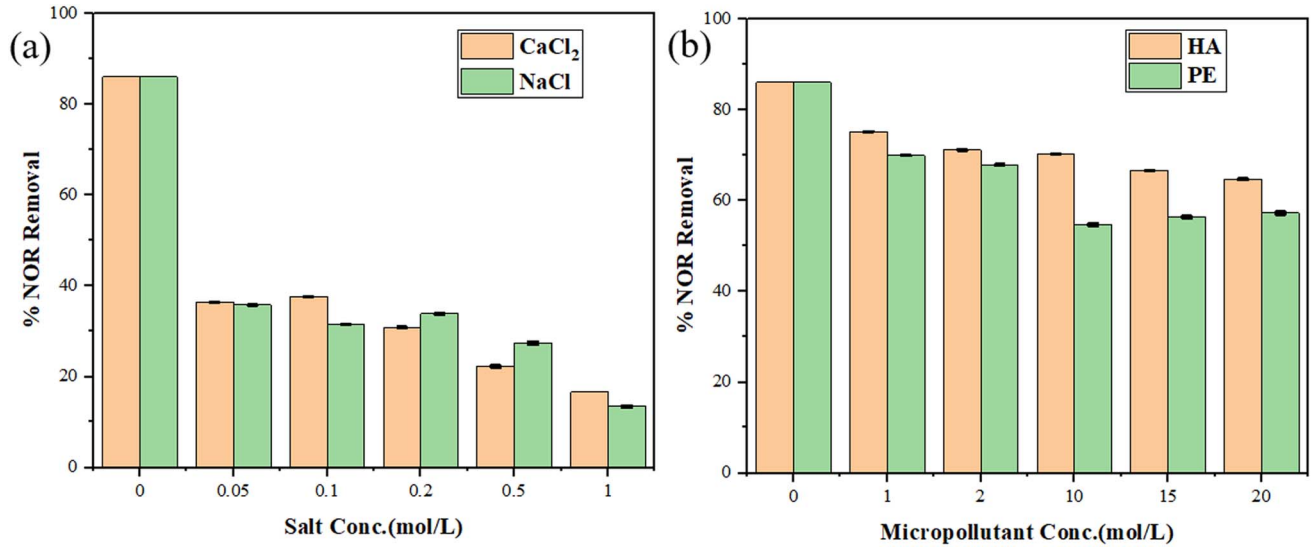

Fig. 5 Environmental factors (a) effects of ionic strength NaCl and $CaCl_2$ (optimized condition: C_{NOR} 20 mg L^{-1}; C_{SOR} 0.15 g L^{-1}; pH 6; contact time 300 min and salt conc. 0–1 mol L^{-1}) (b) effects of environmental micropollutants (optimized condition: C_{NOR} 20 mg L^{-1}; C_{SOR} 0.15 g L^{-1}; pH 6; contact time 300 min and HA and PE conc. 0–20 mol L^{-1}).

of NOR by NBs in order to fully understand the interfacial mechanism underlying the NBs' removal of NOR Fig. 5b illustrates how the HA molecules in the solution affects the rate of NOR removal. The NOR removal rate by NBs is more than 80% when the dosage of HA in the solution is less than 1 mol L^{-1}; however, as the increasing dosage of HA to 20 mol L^{-1}, the adsorption of NOR by NBs drops to 60%.It shows that when the concentration of HA is low, NBs have enough vacant sites to adsorb HA and NOR. As the concentration of HA increased, HA entered the pore filling of NBs and adsorbed on them through the π–π interaction, taking up part of the NBs' active adsorption sites and restricting the amount of NOR that NBs could remove.[37]

3.3 Removal mechanism

For NBs based NOR removal processes, adsorption mechanisms had been crucial. Both chemical and physical adsorption is frequently involved in the adsorption process. The adsorption mechanism of NOR onto NBs was investigated through the analysis of FT-IR and XPS of treated NBs, and the TOC and HR-LCMS tests were employed to investigate the fate of any remaining NOR. According to the adsorption kinetics and isotherm study, adsorption is more consistent with PFO kinetics, and the Langmuir model suggests that monolayer adsorption chemistry serves as the primary basis for adsorption. The investigation into how pH affects NOR adsorption reveals that electrostatic attraction is one of the vital factor influence NOR removal.[13] Further, to clearly understand more about the adsorption mechanism, an XPS analysis was done. In the C 1s spectrum (Fig. 6a and b), the NBs exhibits peaks at 284.4 eV, 285.9 eV, and 287.45 eV, were attributed to the C–C/C=C, C–C, and C=O carbon functional groups. These peaks moved to either higher valence energies or lower binding energies after the NOR adsorption. The shift can be explained by the π–π interactions with the imidazole group on NBs through the conjugated benzene-ring structures and numerous phenolic hydroxyl groups found in NOR. The characteristic peak of O 1s (Fig. 6c and d) can be separated into two groups at 531.08 and 532.44 eV corresponds to C=O/Al–O–Si and C–O. The BE of C 1s and O 1s characteristic peaks shifted after NOR adsorption, mainly for O 1s peak. In addition, there was a significant drop in the C=O/Al–O–Si peak intensity at 531.08 eV. The findings suggested that the hydrogen bonding and complexation processes are the main approaches in the NOR adsorption.[30]

The effect of hydrogen bonding, π–π interaction and amide bonding between NOR and NBs were clearly shown in the FTIR spectrum of treated NBs sample. Fig. 7a shows the treated NBs' FTIR spectrum. On the FT-IR, two new absorption bands (1274 cm^{-1} and 978 cm^{-1}) that corresponded to the –C–F and –N–H stretching vibrations were detected, indicating that NOR had been successfully adsorbed on NBs. Both hydrogen bonding and electrostatic attraction are primarily responsible for the adsorption. The electrostatic interaction between the positively charged nitrogen of the piperazinyl group ($–NH^{2+}$) of NOR and the deprotonated carboxylic acid groups (–COO–) of NBs can be seen by the peak shift of –COO– at 1630 cm^{-1} and 1424 cm^{-1} to 1625 cm^{-1} and 1423 cm^{-1}. Hydrogen bonding was generated by the free electronic pairs of NOR and surface oxygen groups of NBs. It induced the peak of –OH to move from 1035 cm^{-1} to 1033 cm^{-1} and the peak of –COOH (1736 cm^{-1}) to drop.[7]

The TOC estimation of the treated solution aimed to differentiate the roles of adsorption and degradation in NOR removal by NBs (Fig. 7b). The results showed that after 300 minutes, 72.84% of the TOC was removed, whereas 86.06% of the NOR was removed. The inconsistency between the two curves was attributed to the complete degradation of NOR into smaller molecules taking some time.[38] However, the results indicated that adsorption also played a role in NOR removal, as evidenced

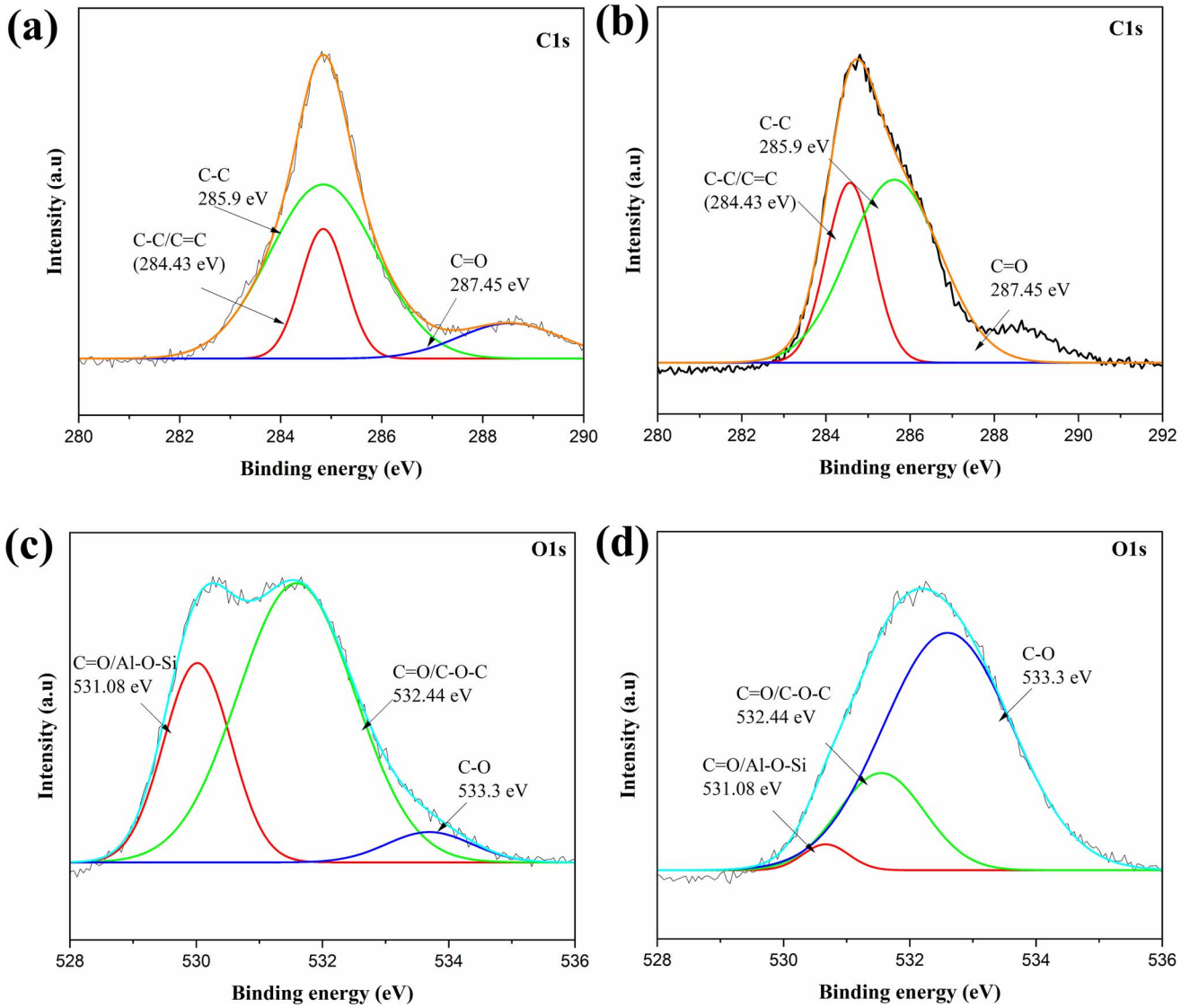

Fig. 6 XPS analysis of NOR interacted NBs (a and b) before and after treated NBs C 1s spectrum (c and d) before and after treated NBs O 1s spectrum.

by the decrease in TOC during the reaction. This indicates that both adsorption and degradation were involved in removing NOR. The linear decreases of TOC concentrations in the residual NOR solution remained low, indicating that the reactive molecules on the NBs surface completely mineralized these intermediates into low-molecular by-products like CO_2 and H_2O.[39]

In order to identify intermediates and analyze potential degradation pathways, LC-MS was employed and the possible intermediates were mentioned in Fig. 7c. NOR (m/z = 320) underwent demethylation, defluorination, piperazine ring opening, and oxidation reactions to become P1 (m/z = 194), which was then further broken down to P2 (m/z = 150) by the decarbonylation reaction. Ultimately, the above products are broken down into smaller molecules like CO_2, H_2O, F^-, and NO_3 by the catalytic processes aided by Fe/Cu bimetal present in the NBs active sites. From, The aforementioned analysis results us to the conclusion that electrostatic interaction, complexation reactions, H bond interactions, π–π stacking interactions, and pore filling were the main causes of the NOR absorption by the NBs.[40]

3.4 Environmental sustainability study

3.4.1 Reusability study. The reusability of the adsorbent is a key consideration when assessing the adsorbents in terms of economic and cost-effectiveness. 0.15 g of NBs and 100 mL of a 20 mg L^{-1} NOR solution were utilized for this purpose. The adsorbents were utilized in the subsequent cycle after being washed with ethanol and dried in a vacuum oven that follows adsorption. The findings demonstrated that the adsorbent could be used for five cycles without causing the adsorbent composite to degrade and with a minimal reduction in NOR adsorption efficiency (Fig. 8a).[25]

3.4.2 Toxicity study. With the goal of investigating the bio toxicity of the degradation products, we conducted culture experiments on the algae *Scenedesmus* sp. The experiments were

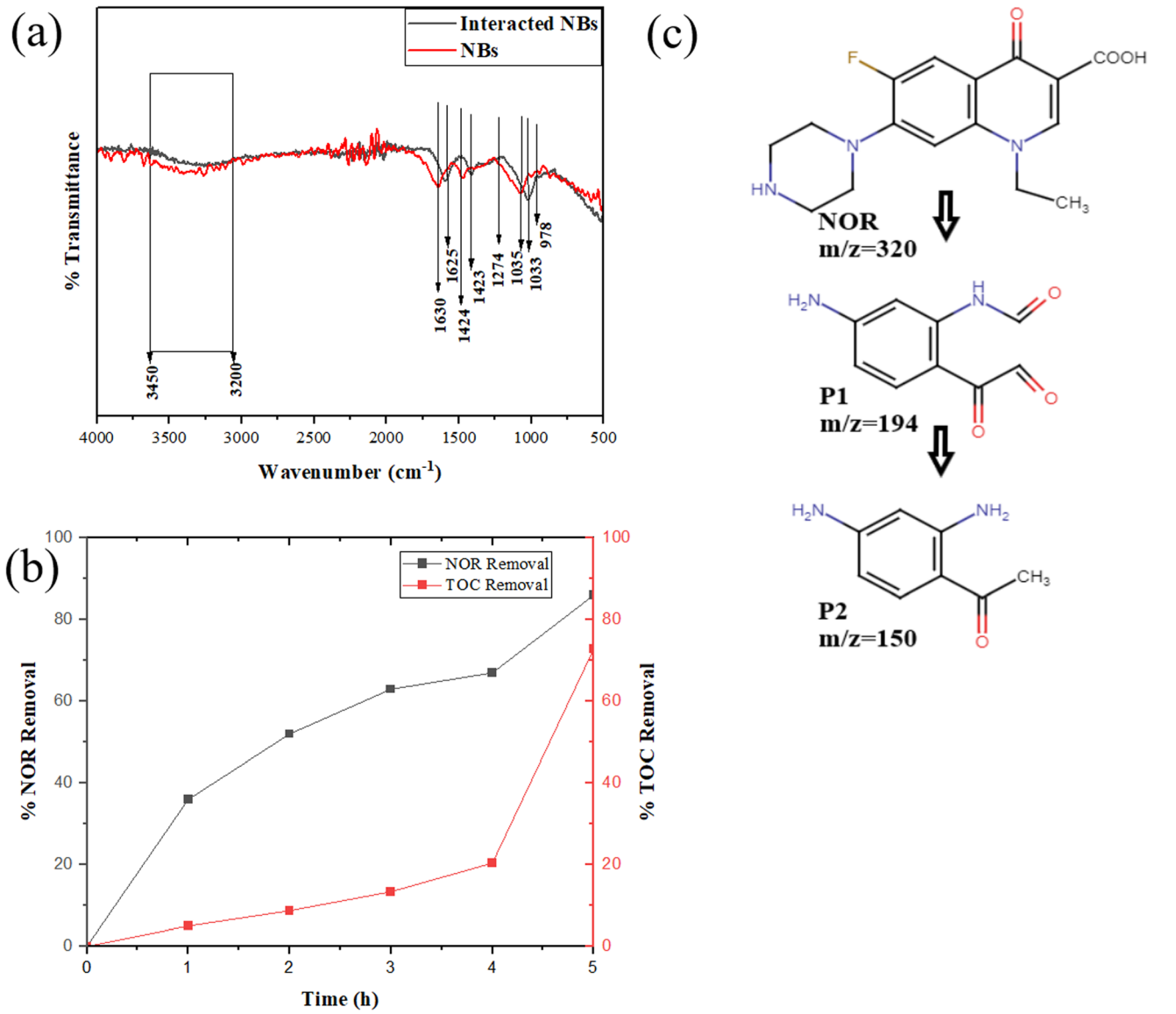

Fig. 7 (a) FTIR analysis of before and after treated NBs (b) % TOC removal efficiency of treated NOR solution (c) possible NOR degradation intermediates.

carried out by adding the NOR (20 mg L^{-1}), treated NOR solution, synthetic wastewater and treated synthetic wastewater. Fig. 6 displays the cell viability results for each treated as well as the control solution. *Scenedesmus* algae were found to have a 77% cell viability when interacting with pollutant solutions treated with NC beads, compared to 36% in the NOR control (Fig. 8b). It is noteworthy that the toxicity value of the treated NOR sample was approximately reduced by half compared to that of the untreated NOR solution. These results confirm the notable effectiveness of the NOR removal technique based on NBs. It is clear that the NOR molecule and intermediate products are oxidized and reduced during this process to produce the least hazardous components possible. Furthermore, even though the treated simulated wastewater contains a variety of organic and inorganic compounds, its toxicity is significantly reduced. The results of these studies indicate that by creating an appropriate eco-friendly solution, it is possible to reduce the residual toxicity of these contaminants.[41]

3.4.3 Effect on real water samples. Based on the intricacy and concentration of the ions, the actual water samples were chosen for this investigation.In addition to Ca^{2+} and Na^{+}, other ions found in river water include K^{+}, Mg^{2+}, HCO_3^{-}, SO_4^{2-}, Cl^{-}, NO_3^{-}, and organic matter. Some of the ions mentioned above can also be found in household tap water, although they are not as concentrated as they are in river water. As displayed in Fig. 8c, the removal potential of adsorbent ranged from 24 to 28% attributed to the limitation of ions to the NOR adsorption capacity of the NBs. Lake water was the most affected of the three water sources selected, according to the study, followed by ground and tap water. Increased pollution in the water would have a greater impact on NB's adsorption capacity. However, the amount of antibiotics in actual wastewater is at ppb levels and

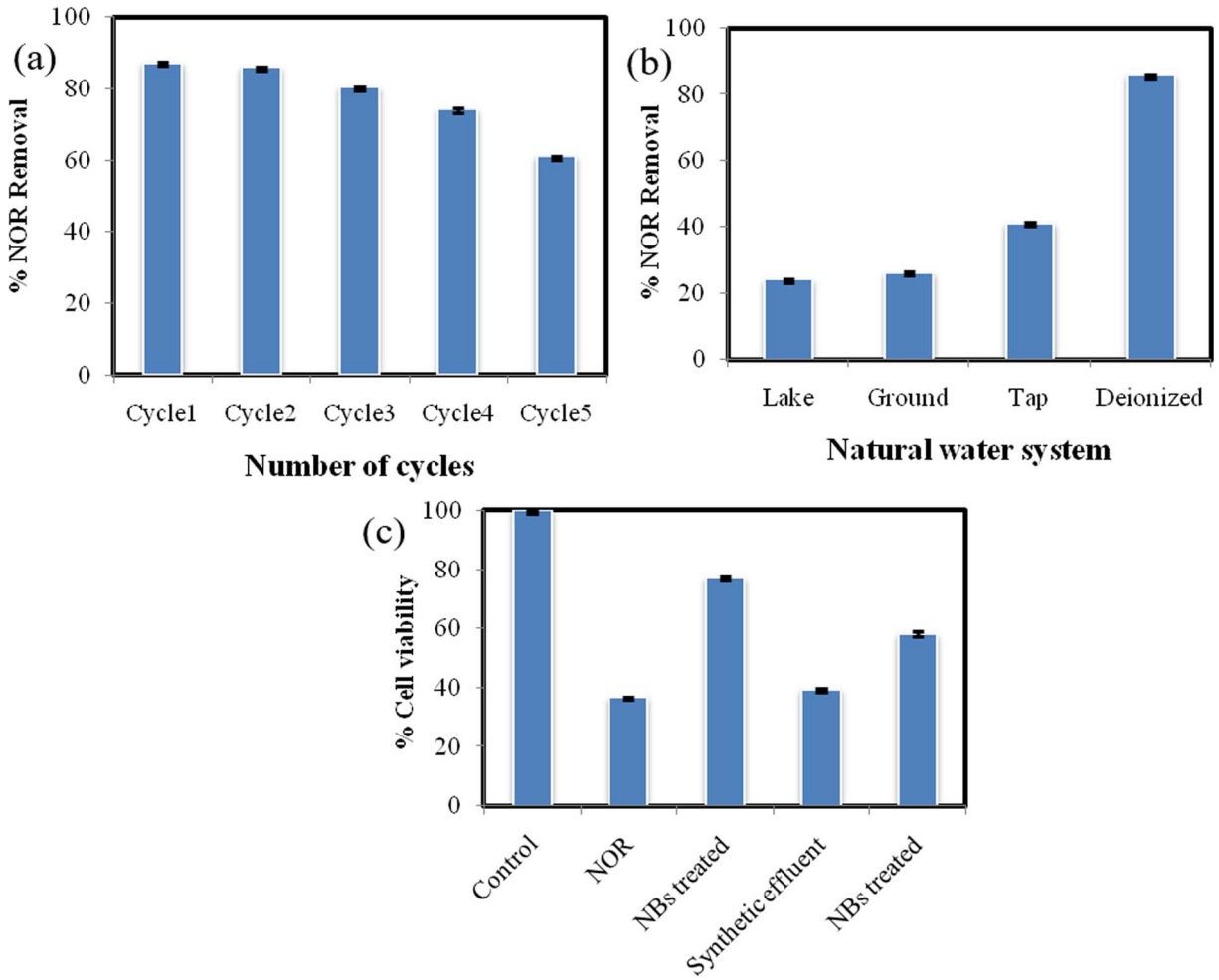

Fig. 8 (a) Reusability study (b) effect on natural watersystem (c) residual toxicity analysis (optimized condition: C_{NOR} 20 mg L^{-1}; C_{SOR} 0.15 g L^{-1}; pH 6; and contact time 300 min).

Table 4 Performance comparison of NBs and other reported nanocomposite hydrogel beads

Adsorbent	Adsorbent type	Experimental condition	Removal (% or mg g^{-1})	References
MagFePC/SA	Hydrogel bead	C_{NOR} = 10 mg L^{-1}, pH = 7.0, T = 25 °C, C_{AT} = 50g L^{-1}, H_2O_2 = 600 μL	96.3%	25
CA/CTS-M	Hydrogel spheres	C_{NOR} = 200 mg L^{-1}, C_{Sor} = 0.5 g L^{-1}, time = 2 h, pH = 6	310.6 mg g^{-1}	13
CG/Bx/ZnO	Hydrogel spheres'	C_{NOR} = 20 mg L^{-1}, C_{Sor} = 10 mg L^{-1}, time = 8 h, pH = 4	99.4%	26
HAP@CT	Nanocomposite	C_{NOR} = 100 mg L^{-1}, C_{Sor} = 0.5 g L^{-1}, time = 120 min, pH = 7	92%	43
Nat-HAp	Nanocomposite	C_{NOR} = 132.57 mg L^{-1}, C_{Sor} = 0.99 g L^{-1}, time = 120 min, pH = 7.88	96.20%	7
GOMBt	Granular nanocomposite	C_{NOR} = 3 mg L^{-1}, C_{Sor} = 0.1 g L^{-1}, time = 24 h, pH = 5	3.846 mg g^{-1}	35
NBs	Hydrogel beads	C_{NOR} = 20 mg L^{-1}, C_{Sor} = 0.15g L^{-1}, time = 300 min, pH = 6	354.9 ± 41 mg g^{-1}	This study

significantly lowers than the NOR concentration range examined here, yet NBs also exhibit effective adsorption to wastewater. Indeed, more than 70% of the NBs in the stimulated wastewater could be removed. As a result, NBs are thought to be promising potential adsorbents for a variety of aqueous solutions.[42]

3.4.4 Comparison study. Table 4 compares the maximum NOR adsorption capacity of a few different adsorbents. Among the number of adsorbent materials previously stated, it was evident that the NBs (354.9 mg g^{-1}) had the highest adsorption capacity. For this reason, NBs can be regarded as an excellent and sustainable adsorbent for removing NOR from aqueous solutions.

4. Conclusion

We have successfully investigated the removal efficiency of NBs against the antibiotic pollutant NOR in this work. With the optimal conditions of C_{Nor} 20 mg L^{-1}, C_{sor} 0.15 g L^{-1}, pH 6, and contact time of 300 min, it shows the NOR removal percentage of >86%. Furthermore, NBs showed increased selectivity toward NOR even when NaCl, $CaCl_2$, HA, and polyethylene were present. Even in different real water sources, NBs continued to show good adsorption ability toward NOR. NBs adsorption isotherms and kinetics fit the Langmuir model and the PFO, which depict the monolayer physisorption process quite well. In addition to the examination of the adsorption thermodynamics, the adsorption of NOR on NBs was determined to be an endothermic, spontaneous reaction. In comparison to most previously reported adsorbents, the theoretical maximum adsorption capacity of NBs for NOR is 355 mg g^{-1}. Moreover, NBs have a high recovery capacity and can be used as a cyclic adsorption material for NOR adsorption; recovery occurs after five adsorption and desorption steps. Hence, NBs, which are easy to synthesis, recycle, and ecologically beneficial, have a promising future in environmental adsorption.

Conflicts of interest

There are no conflicts to declare.

Acknowledgements

This work was supported by the Department of Science and Technology (DST) INSPIRE fellowship for Selected Research Scholars of India (Grant No: IF190196).

References

1 J. Du, Q. Liu, Y. Pan, S. Xu, H. Li and J. Tang, *Antibiotics*, 2023, 12.
2 D. G. J. Larsson, C. de Pedro and N. Paxeus, *J. Hazard. Mater.*, 2007, **148**, 751–755.
3 R. Ricky and S. Shanthakumar, *Sci. Rep.*, 2023, **13**, 13911.
4 J. Georgin, D. S. P. Franco, L. Meili, A. Bonilla-Petriciolet, T. A. Kurniawan, G. Imanova, E. Demir and I. Ali, *Adv. Colloid Interface Sci.*, 2024, **324**, 103096.
5 Y. Pan, J. Dong, L. Wan, S. Sun, H. J. MacIsaac, K. G. Drouillard and X. Chang, *J. Hazard. Mater.*, 2020, **385**, 121625.
6 P. Li, C.-Z. Chen, X.-L. Zhao, L. Liu and Z.-H. Li, *Chemosphere*, 2023, **325**, 138389.
7 S. Cheikh, A. Imessaoudene, J.-C. Bollinger, A. Manseri, A. Bouzaza, A. Hadadi, N. Hamri, A. Amrane and L. Mouni, *J. Mol. Liq.*, 2023, **392**, 123424.
8 M. B. Ahmed, J. L. Zhou, H. H. Ngo and W. Guo, *Sci. Total Environ.*, 2015, **532**, 112–126.
9 P. Chang, Z. Li, W. Jiang and B. Sarkar, *Chapter 7. Clay Minerals for Pharmaceutical Wastewater Treatment*, Elsevier Inc., 2019.
10 Y. Liu, S. Zhu, B. Zhao, J. Ai and Z. Liu, *Mater. Lett.*, 2021, **290**, 129478.
11 H. Zhou, Z. Wang, C. Gao, Q. Sun, J. Liu and D. She, *Bioresour. Technol.*, 2023, **369**, 128402.
12 X. Cao, Z. Meng, E. Song, X. Sun, X. Hu, W. Li, Z. Liu, S. Gao and B. Song, *Chemosphere*, 2022, **299**, 134414.
13 J. Tang, L. Wang, W. Qin, Z. Qing, C. Du, S. Xiao and B. Yan, *Chemosphere*, 2023, **335**, 139048.
14 L. Chen, Y. Zhao, Y. Miao, M. Li, H. Bai, S. Song and T. Zhang, *J. Mol. Liq.*, 2024, **396**, 124016.
15 A. S. Abdul Rahman, A. N. S. Fizal, N. A. Khalil, A. N. Ahmad Yahaya, M. S. Hossain and M. Zulkifli, *Polymers*, 2023, **15**(11), 2494.
16 X. Wang, B. Liu, Z. Liu, J. Li, R. Lu, H. Gao, C. Pan and W. Zhou, *Int. J. Biol. Macromol.*, 2024, **260**, 129127.
17 G. Gopal, H. Sankar, C. Natarajan and A. Mukherjee, *J. Environ. Manage.*, 2020, **254**, 109812.
18 G. G. Hacıosmanoğlu, C. Mejías, J. Martín, J. L. Santos, I. Aparicio and E. Alonso, *J. Environ. Manage.*, 2022, **317**, 115397.
19 I. A. Ahmed, H. S. Hussein, Z. A. ALOthman, A. G. ALanazi, N. S. Alsaiari and A. Khalid, *Polymers*, 2023, **15**(5), 1221.
20 G. Gopal, M. J. Nirmala and A. Mukherjee, *Surf. Interfaces*, 2023, **39**, 102981.
21 G. Gopal, C. Natarajan and A. Mukherjee, *Environ. Technol. Innovation*, 2022, **28**, 102783.
22 S. J. Peighambardoust, O. Aghamohammadi-Bavil, R. Foroutan and N. Arsalani, *Int. J. Biol. Macromol.*, 2020, **159**, 1122–1131.
23 K. V. G. Ravikumar, H. Kubendiran, K. Ramesh, S. Rani, T. K. Mandal, M. Pulimi, C. Natarajan and A. Mukherjee, *Environ. Technol. Innovation*, 2020, **17**, 100520.
24 A. A. H. Faisal, A. H. Shihab, M. Naushad, T. Ahamad, G. Sharma and K. M. Al-Sheetan, *J. Environ. Chem. Eng.*, 2021, **9**, 105342.
25 D. Liu, W. Gu, W. Zhou, Y. Xu, W. He, L. Liu, L. Zhou, J. Lei, J. Zhang and Y. Liu, *J. Cleaner Prod.*, 2022, **369**, 133239.
26 P. Sharma, M. Sharma, H. Laddha, R. Gupta and M. Agarwal, *Int. J. Biol. Macromol.*, 2023, **238**, 124145.
27 J. He, Z. Jiang, X. Fu, F. Ni, F. Shen, S. Zhang, Z. Cheng, Y. Lei, Y. Zhang and Y. He, *Ecotoxicol. Environ. Saf.*, 2023, **251**, 114521.
28 G. Che, Q. Zhang, L. Lin, W. Chen and X. Li, *Environ. Sci. Pollut. Res.*, 2020, **27**, 35638–35649.
29 M. H. Al-Jabari, S. Sulaiman, S. Ali, R. Barakat, A. Mubarak and S. A. Khan, *J. Mol. Liq.*, 2019, **291**, 111249.
30 Y. Lan, Y. Luo, S. Yu, H. Ye, Y. Zhang, M. Xue, Q. Sun, Z. Yin, X. Li, C. Xie, Z. Hong and B. Gao, *Sep. Purif. Technol.*, 2024, **330**, 125543.

31 L. N. Shi, Y. Zhou, Z. Chen, M. Megharaj and R. Naidu, *Environ. Sci. Pollut. Res.*, 2013, **20**, 3639–3648.
32 N. Marsiezade and V. Javanbakht, *Int. J. Biol. Macromol.*, 2020, **162**, 1140–1152.
33 S. Altaf, R. Zafar, W. Q. Zaman, S. Ahmad, K. Yaqoob, A. Syed, A. J. Khan, M. Bilal and M. Arshad, *Ecotoxicol. Environ. Saf.*, 2021, **226**, 112826.
34 Y. Zhou, Y. He, Y. He, X. Liu, B. Xu, J. Yu, C. Dai, A. Huang, Y. Pang and L. Luo, *Sci. Total Environ.*, 2019, **650**, 2260–2266.
35 J. Zhou and Q. Sun, *Polymers*, 2022, **14**(19), 3984.
36 Z. Zhang, H. Liu, H. Wen, L. Gao, Y. Gong, W. Guo, Z. Wang, X. Li and Q. Wang, *Sci. Total Environ.*, 2021, **798**, 149344.
37 F. Tahmasebi, M. Alimohammadi, R. Nabizadeh, M. Khoobi, K. Karimian and A. Zarei, *Korean J. Chem. Eng.*, 2019, **36**, 894–902.
38 J. Wu, T. Wang, Y. Liu, W. Tang, S. Geng and J. Chen, *Chemosphere*, 2022, **303**, 135264.
39 K. V. G. Ravikumar, S. V. Sudakaran, K. Ravichandran, M. Pulimi, C. Natarajan and A. Mukherjee, *J. Cleaner Prod.*, 2019, **210**, 767–776.
40 X. Chen and J. Wang, *Chem. Eng. J.*, 2020, **395**, 125095.
41 K. V. G. Ravikumar, G. Debayan, P. Mrudula, N. Chandrasekaran and A. Mukherjee, *Front. Environ. Sci. Eng.*, 2020, **14**, 1–13.
42 S. Manna, P. Das, P. Basak, A. K. Sharma, V. K. Singh, R. K. Patel, J. K. Pandey, V. Ashokkumar and A. Pugazhendhi, *Chemosphere*, 2021, **280**, 130961.
43 A. Nayak, B. Bhushan and S. Kotnala, *Mater. Today: Proc.*, 2022, **61**, 143–149.